5-1-2024

Spatial mapping of hematopoietic clones in human bone marrow

Andrew L Young
Washington University School of Medicine in St. Louis
Hannah C Davis
Washington University School of Medicine in St. Louis
Maggie J Cox
Washington University School of Medicine in St. Louis
Tyler M Parsons
Washington University School of Medicine in St. Louis
Samantha C Burkart
Washington University School of Medicine in St. Louis

See next page for additional authors

RESEARCH BRIEF

Spatial Mapping of Hematopoietic Clones in Human Bone Marrow

Andrew L. Young[1], Hannah C. Davis[2], Maggie J. Cox[1], Tyler M. Parsons[2], Samantha C. Burkart[2], Diane E. Bender[3], Lulu Sun[4], Stephen T. Oh[1], and Grant A. Challen[2]

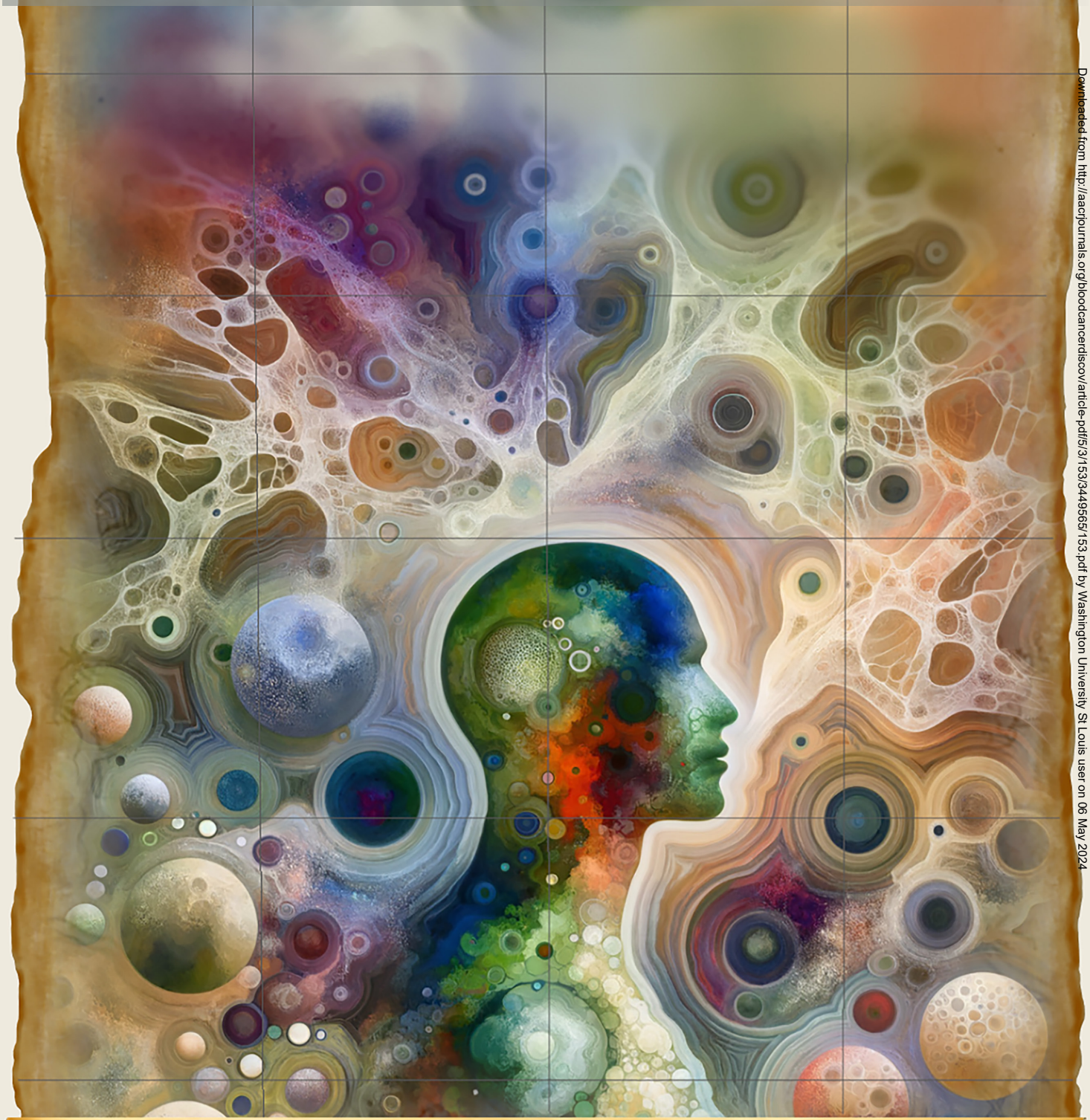

ABSTRACT Clonal hematopoiesis (CH) is the expansion of somatically mutated cells in the hematopoietic compartment of individuals without hematopoietic dysfunction. Large CH clones (i.e., >2% variant allele fraction) predispose to hematologic malignancy, but CH is detected at lower levels in nearly all middle-aged individuals. Prior work has extensively characterized CH in peripheral blood, but the spatial distribution of hematopoietic clones in human bone marrow is largely undescribed. To understand CH at this level, we developed a method for spatially aware somatic mutation profiling and characterized the bone marrow of a patient with polycythemia vera. We identified the complex clonal distribution of somatic mutations in the hematopoietic compartment, the restriction of somatic mutations to specific subpopulations of hematopoietic cells, and spatial constraints of these clones in the bone marrow. This proof of principle paves the way to answering fundamental questions regarding CH spatial organization and factors driving CH expansion and malignant transformation in the bone marrow.

SIGNIFICANCE: CH occurs commonly in humans and can predispose to hematologic malignancy. Although well characterized in blood, it is poorly understood how clones are spatially distributed in the bone marrow. To answer this, we developed methods for spatially aware somatic mutation profiling to describe clonal heterogeneity in human bone marrow.

See related commentary by Austin and Aifantis, p. 139.

INTRODUCTION

All humans become mosaics over time as somatic stem cells acquire genetic mutations throughout life (1, 2). In the hematopoietic compartment, this leads to the condition termed clonal hematopoiesis (CH) when specific mutations (e.g., *JAK2* V617F) provide a competitive advantage without evidence of overt hematologic dysfunction (3). These hematopoietic clones are long-lived, arise from hematopoietic stem and progenitor cells (HSPC), and often expand over time (4, 5). CH increases in prevalence with age and is associated with an increased risk for hematologic malignancy and all-cause mortality (6–8). The mutations observed in CH strongly overlap with those observed in hematologic malignancies (9, 10). Although CH is universal, little is known about the nongenetic intrinsic and extrinsic factors driving clonal evolution and malignant transformation.

Prior work has shown that clonal mutations in solid organs such as skin and esophagus are spatially constrained (1, 2). However, in the hematopoietic compartment, the spatial organization of clones harboring leukemia-associated somatic mutations and their interaction with the niche and each other is largely unknown. To explore this, we developed methods to describe the clonal distribution in the bone marrow contained within a femur head explant. Hip arthroplasty is a common surgical procedure in the elderly and provides a readily accessible window into the hematopoietic system. Prior work has examined the incidence of CH in patients undergoing hip arthroplasty, which identified a relatively high incidence of CH at 50% in this older population and a possible connection to autoimmune disease (11). A subsequent study of CH in patients with osteoarthritis undergoing hip arthroplasty demonstrated that CH clones detected in the femur head explant obtained during arthroplasty were undetectable in the peripheral circulation after arthroplasty—suggesting a spatial constraint for the CH clone in the femur head (12). Although this prior study isolated bulk bone marrow cells from the entire femur head, we present an approach to provide millimeter-level resolution for the spatial distribution of hematopoietic clones within the bone marrow.

As proof of principle, we characterized the hematopoietic clonal distribution within a femur head explant from a 50-year-old man with polycythemia vera (PV). PV is a myeloproliferative neoplasm (MPN) driven by the activating *JAK2* V617F mutation in more than 90% of cases. This mutation is also found in approximately 5% of individuals with CH (4, 13, 14). There is increasing evidence that the clonal mutations driving MPNs arise early in life, potentially *in utero*, years before the manifestation of symptoms (15). We chose this patient for a proof-of-principle study because of the clonal complexity and high mutant cell burden often found within the bone marrow of MPN patients. We hypothesized that the hematopoietic clones would be geographically constrained in distinct niches within the bone marrow of this patient. To test this hypothesis, we performed bulk genomic sequencing, droplet digital PCR (ddPCR) validation, spatially aware variant detection, single-cell sequencing, and longitudinal tracking of clonal mutations over time.

RESULTS

Patient Information and Bulk Characterization of Hematopoietic Clones

A 50-year-old man (UPN978825) with PV undergoing planned hip arthroplasty was selected for bone marrow clonal

[1]Division of Hematology, Department of Medicine, Washington University School of Medicine, St. Louis, Missouri. [2]Division of Oncology, Department of Medicine, Washington University School of Medicine, St. Louis, Missouri. [3]The Bursky Center for Human Immunology and Immunotherapy Programs Immunomonitoring Laboratory, Washington University School of Medicine, St. Louis, Missouri. [4]Department of Pathology and Immunology, Washington University School of Medicine, St. Louis, Missouri.

Corresponding Author: Grant A. Challen, Washington University School of Medicine, 660 Euclid Avenue, St. Louis, MO 63110. E-mail: grantchallen@wustl.edu

Blood Cancer Discov 2024;5:153–63

doi: 10.1158/2643-3230.BCD-23-0110

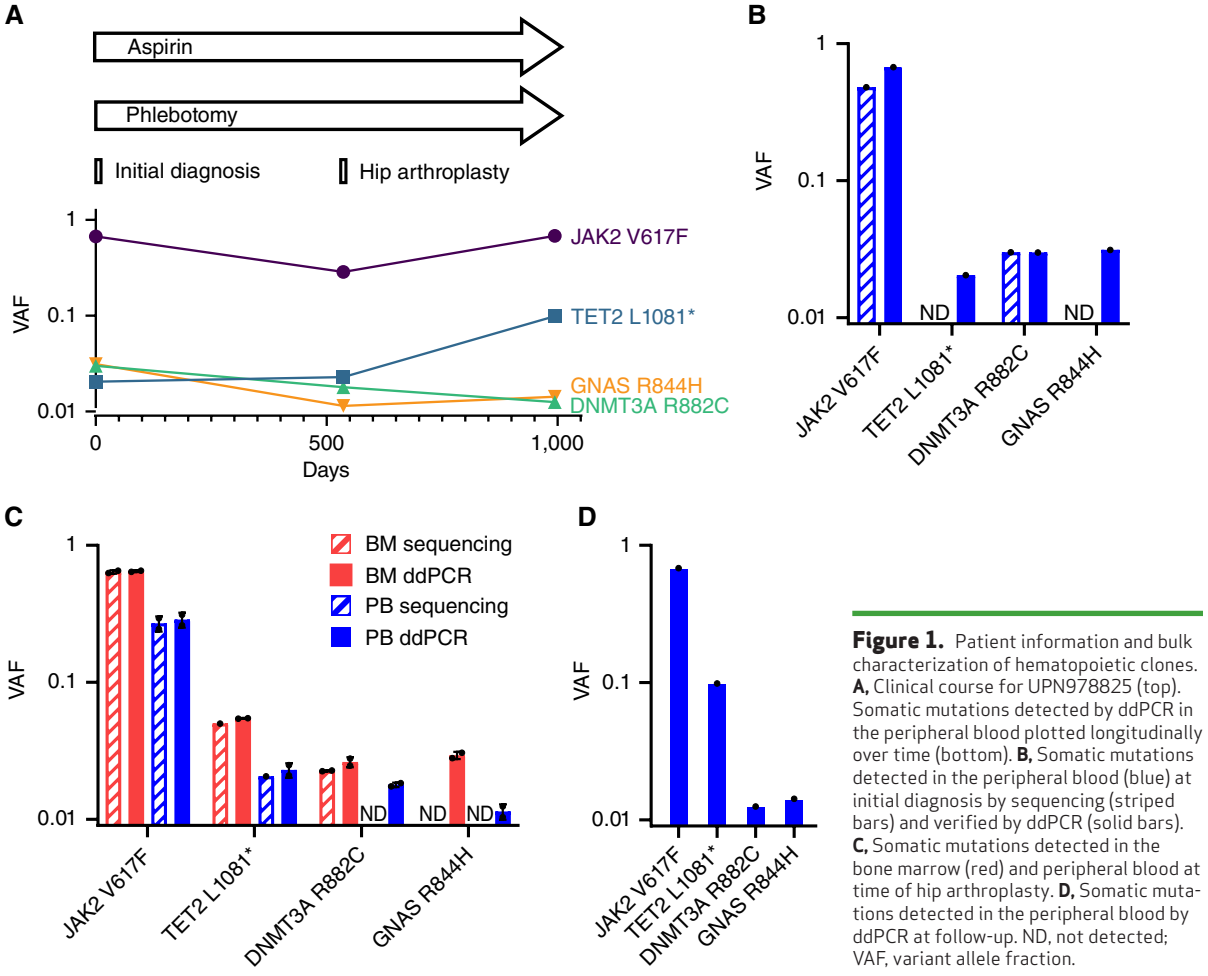

Figure 1. Patient information and bulk characterization of hematopoietic clones. **A,** Clinical course for UPN978825 (top). Somatic mutations detected by ddPCR in the peripheral blood plotted longitudinally over time (bottom). **B,** Somatic mutations detected in the peripheral blood (blue) at initial diagnosis by sequencing (striped bars) and verified by ddPCR (solid bars). **C,** Somatic mutations detected in the bone marrow (red) and peripheral blood at time of hip arthroplasty. **D,** Somatic mutations detected in the peripheral blood by ddPCR at follow-up. ND, not detected; VAF, variant allele fraction.

architecture characterization and longitudinal peripheral blood mutation tracking (Fig. 1A). The patient initially presented with abdominal discomfort, fatigue, and weight loss. He was found to have splenomegaly on abdominal imaging, and bone marrow biopsy confirmed the diagnosis of PV. Molecular testing of the peripheral blood obtained at diagnosis as standard of care showed a *JAK2* V617F mutation at 0.48 variant allele fraction (VAF) and a *DNMT3A* R882C mutation at 0.03 VAF (Fig. 1B). He was managed conservatively with aspirin and phlebotomy for approximately 1.5 years before undergoing hip arthroplasty for osteoarthritis.

Bulk peripheral blood and bone marrow aspirate mononuclear cells obtained perioperatively during hip arthroplasty were sequenced in duplicate using a targeted, error-corrected myeloid panel (Supplementary Table S1). The bulk bone marrow and peripheral blood specimens were sequenced to 2811-3810x and 3128-3142x coverage across the target space, respectively (Supplementary Table S2). In the bulk bone marrow, *JAK2* V617F and *DNMT3A* R882C mutations were identified at 0.64 and 0.02 VAF, respectively, and a previously undetected *TET2* L1081* mutation was identified at 0.05 VAF (Fig. 1C). In the peripheral blood, the *JAK2* V617F and *TET2* L1081* mutations were detected at 0.27 and 0.02 (one replicate) VAF, respectively, and the *DNMT3A* R882C mutation was not detected (Fig. 1C). These sequencing results were validated by ddPCR (Fig. 1B and C). Additionally, ddPCR confirmed a *GNAS* R844H mutation not identified by bulk sequencing but discovered by single-cell analysis detailed below (Fig. 1B and C). Approximately 15 months after hip arthroplasty, ddPCR analysis of peripheral blood mononuclear cells identified *JAK2* V617F, *TET2* L1081*, *DNMT3A* R882C, and *GNAS* R844H mutations at 0.68, 0.10, 0.012, and 0.014 VAF, respectively (Fig. 1D). These clonal mutations showed variable evolution in the peripheral blood over time with the *JAK2* V617F and *TET2* L1081* mutations increasing after hip arthroplasty (Fig. 1A).

Single-Cell DNA Sequencing and Immunophenotyping to Resolve Clonal Hierarchy

Bone marrow mononuclear cells were subjected to single-cell targeted DNA sequencing and immunophenotyping using the Mission Bio Tapestri platform (Supplementary Table S3). In total, 1,486 high-quality cells were analyzed with an average of 129x coverage per cell per amplicon for genomic mutations and 300x coverage per cell per antibody tag. Analysis identified the *JAK2* V617F, *DNMT3A* R882C, and *TET2* L1081* mutations identified previously, as well as a previously undetected *GNAS* R844H mutation (Fig. 2A). The single-cell analysis disentangled the clonal complexity of this patient's disease—a large *JAK2* V617F homozygous clone, a small *TET2* L1081* heterozygous subclone, a small *JAK2* V617F heterozy-

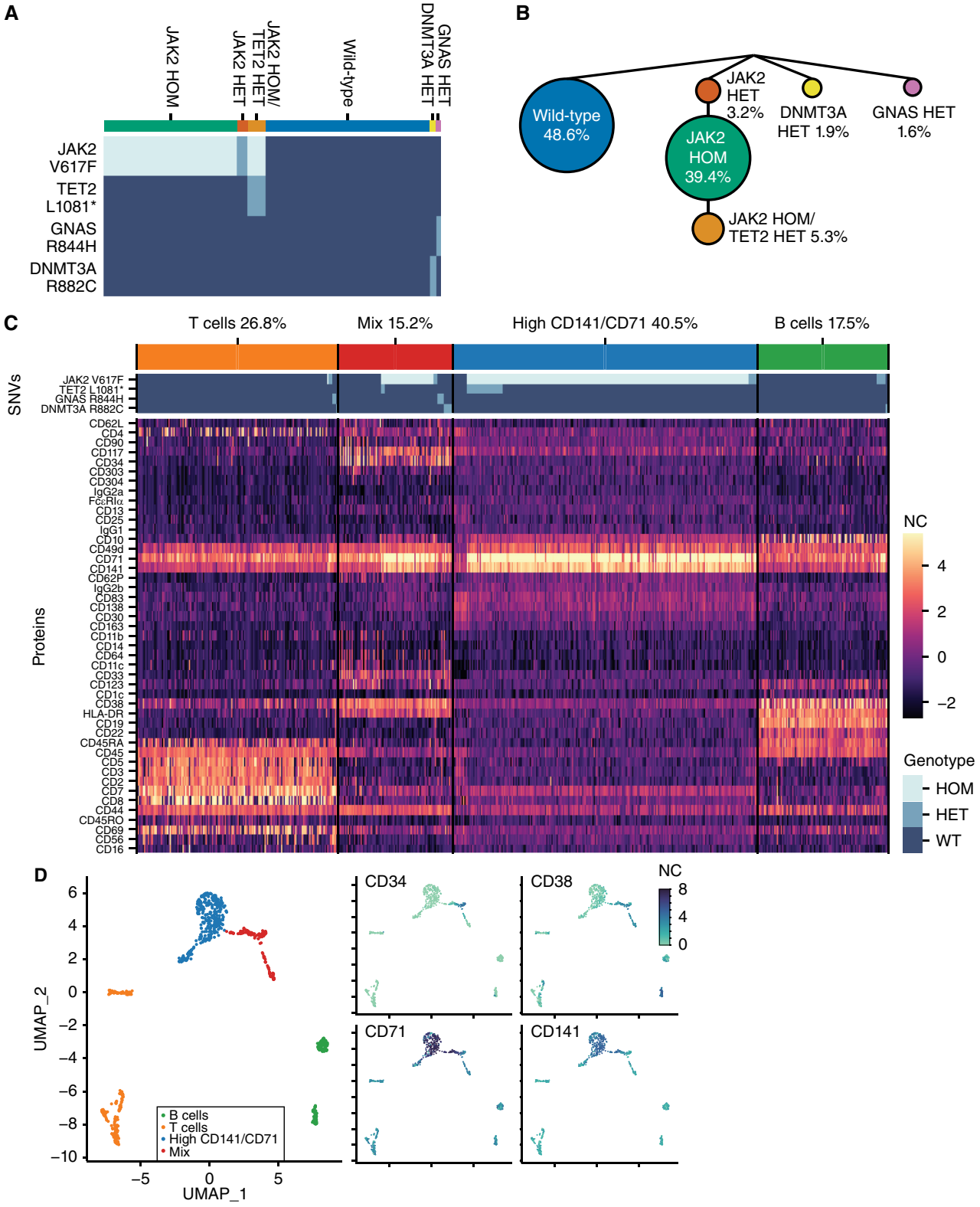

Figure 2. Single-cell DNA sequencing and immunophenotyping to resolve clonal hierarchy. **A,** Somatic mutations detected in each single-cell isolated from bone marrow and clustered by mutation profile. **B,** Clonal hierarchy of bone marrow hematopoietic cells depicting a large population of wild-type cells, *JAK2* V617F heterozygous and homozygous clones with a *TET2* L1081* heterozygous subclone, and independent *GNAS* R844H and *DNMT3A* R882C heterozygous clones. **C,** Immunophenotype profile of individual cells isolated from the bone marrow aspirate and clustered by cell type into $CD3^+$ T cells, $CD19^+$ B cells, a malignant population of cells highly expressing CD141 and CD71, and a mixed population of malignant and nonmalignant progenitor cells. **D,** Clustering of single cells by immunophenotype profile and colored by cell type (left facet) and compared with the relative expression of key hematopoietic markers including CD34, CD38, CD71, and CD141 (right facets). (*continued on following page*)

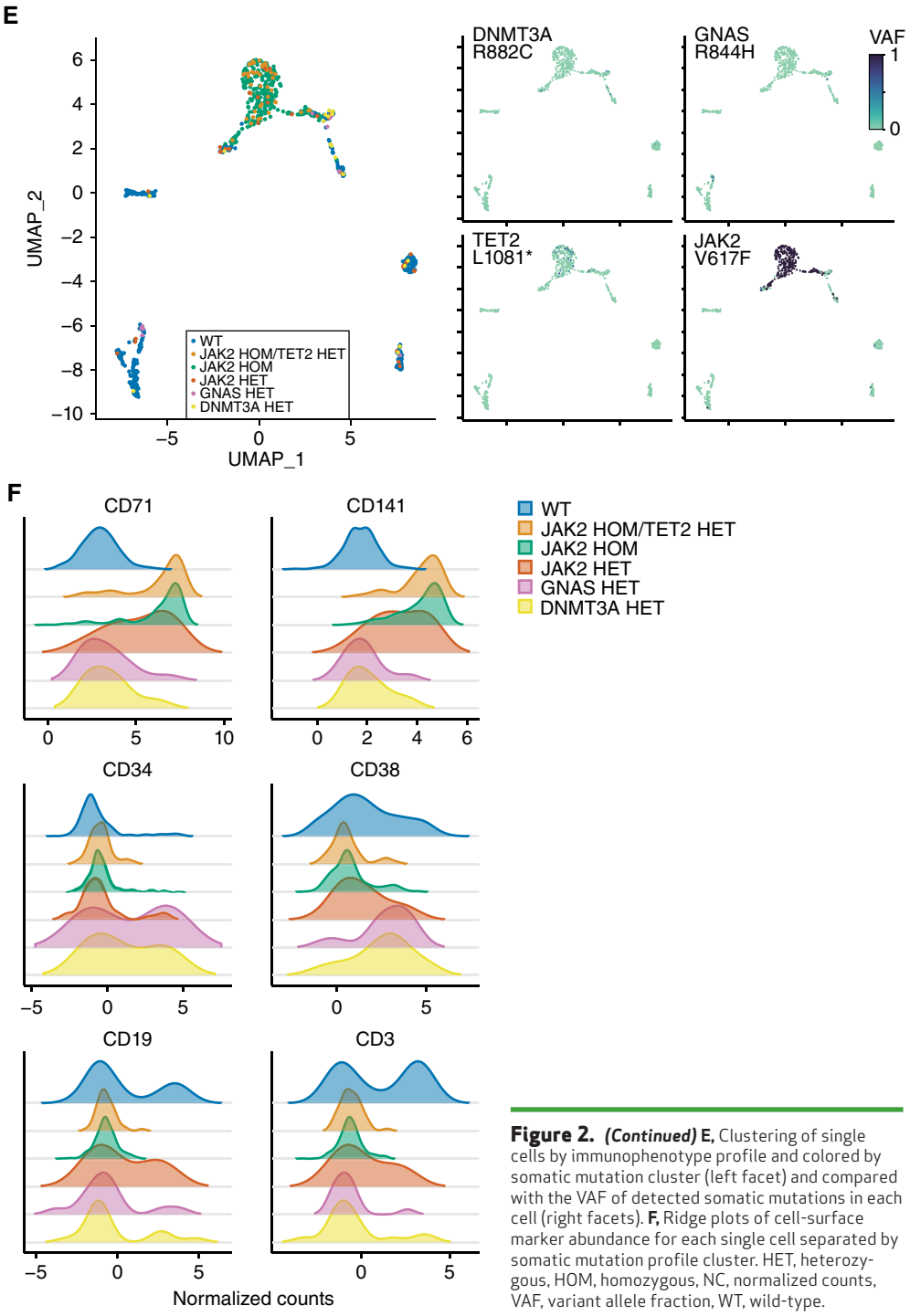

Figure 2. ***(Continued)*** **E,** Clustering of single cells by immunophenotype profile and colored by somatic mutation cluster (left facet) and compared with the VAF of detected somatic mutations in each cell (right facets). **F,** Ridge plots of cell-surface marker abundance for each single cell separated by somatic mutation profile cluster. HET, heterozygous, HOM, homozygous, NC, normalized counts, VAF, variant allele fraction, WT, wild-type.

gous clone, and independent *GNAS* R844H heterozygous and *DNMT3A* R882C heterozygous clones (Fig. 2A). The *GNAS* R844H mutation is a recurrent hotspot mutation frequently observed in pancreatic and gastrointestinal cancers and also observed in hematologic malignancies (16, 17). From these observations, the simplest sequence of mutational events implied that the *JAK2* V617F heterozygous mutation arose first, followed by a second biallelic *JAK2* V617F mutation that expanded significantly, and subsequently acquired a *TET2* L1081* mutation (Fig. 2B).

Single-cell immunophenotyping analysis revealed cell populations in the bone marrow that clustered into four predominant groups including CD19$^+$ B lymphocytes, CD3$^+$ T lymphocytes, a population of cells highly expressing CD141 (thrombomodulin) and CD71 (transferrin receptor 1), and a mixed population of largely CD38$^+$ hematopoietic progenitors (Fig. 2C). Dimensional reduction by uniform manifold approximation and projection (umap) analysis separated the B- and T-lymphocyte populations away from the mixed stem and progenitor and the high CD141/CD71 populations (Fig. 2D;

Supplementary Fig. S1). Combining the genotyping and immunophenotyping single-cell analyses demonstrated that the high CD141/CD71 cluster likely represented the neoplastic clones comprised of the *JAK2* V617F homozygous population and the *TET2* L1081* heterozygous subclone; the lymphoid cells were largely devoid of somatic mutations; and the mixed population (containing the HSPCs) was comprised of *JAK2* homozygous cells, wild-type cells, and the *GNAS* R844H and *DNMT3A* R882C heterozygous clones (Fig. 2C and E).

Overlaying the mutational information on the UMAP demonstrated the overlap between the CD141/CD71 cluster and the *JAK2* V617F homozygous clone and the *TET2* L1081* subclone, the maturation of wild-type hematopoietic progenitor cells, and the maturation of *JAK2* V617F homozygous mutated cells from a CD38-positive progenitor population (Fig. 2D and E). Focusing on the most discriminatory markers reinforced the relationship between CD141/CD71 positivity and *JAK2* V617F mutation status (Fig. 2F). Additionally, the *GNAS* R844H and *DNMT3A* R882C heterozygous mutant cells were largely identified in a progenitor state marked by variable CD34 positivity and uniform CD38 positivity (Fig. 2F). Together, these results describe a complex clonal composition of the patient's hematopoietic compartment where multiple independent hematopoietic clones coevolved simultaneously.

Mutation Detection in HSPC Subpopulations

To validate the single-cell findings and further describe mutation distribution in HSPC subpopulations, $CD71^+$ erythroblasts (Fig. 3A) and distinct HSPC subpopulations (Fig. 3B) were purified by flow cytometry from a separate bone marrow specimen. In these purified cell populations (Supplementary Table S4), the *JAK2* V617F mutation burden was highest in the $CD71^+$ fraction of $CD34^+$ HSPCs (0.41 VAF) and $CD33^+$ myeloid cells (0.57 VAF) and lowest in the $CD71^-$ fraction of $CD34^+$ HSPCs (0.069 VAF) and lymphoid cells (not detected) when assessed by ddPCR (Fig. 3C). From the single-cell sequencing studies, the *TET2* L1081* mutation arose within a hematopoietic cell homozygous for the *JAK2* V617F mutation (Fig. 2A). Interestingly, the *TET2* L1081* mutation was most prevalent in the $CD71^+$ erythroblasts (0.025 VAF) and $CD33^+$ myeloid cells and not detected in the $CD71^-$ fraction of $CD34^+$ HSPCs or lymphoid cells (Fig. 3D). In the $CD33^+$ myeloid cells, increasing expression of CD71 (negative vs. low) was associated with a small increased mutational prevalence of *TET2* L1081* (0.035 vs. 0.067 VAF, respectively; Fig. 3D). The *JAK2* V617F and *TET2* L1081* mutations were not detected in lymphoid cells, suggesting a myeloid-restricted cell of origin. Conversely, the *DNMT3A* R882C and *GNAS* R844H mutations were identified in both myeloid and lymphoid populations (Fig. 3D).

The peripheral blood was largely comprised of $CD33^+$ myeloid cells and $CD3^+$ or $CD19^+$ lymphoid cells with few circulating $CD34^+$ HSPCs or $CD71^+$ erythroblasts (Fig. 3E; Supplementary Table S4). In the peripheral blood, the rare $CD34^+$ HSPCs had high *JAK2* V617F mutation prevalence, which was higher in the $CD71^+$ fraction (0.58 VAF) compared with the $CD71^-$ fraction (0.35 VAF) by ddPCR (Fig. 3F). The *JAK2* V617F mutation was less prevalent in the $CD33^+$ myeloid cells (0.11 VAF) and $CD71^+$ erythroblasts (0.21 VAF) and even less prevalent in lymphoid cells (undetected in T cells and 0.0008 VAF in B cells; Fig. 3F). The *TET2* L1081* mutation was largely restricted to $CD34^+$ HSPCs, $CD33^+$ myeloid cells, and $CD71^+$ erythroblasts and not detected in lymphoid cells in the peripheral blood (Fig. 3G). Similar to the bone marrow, the *GNAS* R844H and *DNMT3A* R882C mutations were detected in HSPCs, myeloid cells, and lymphoid cells in the peripheral blood (Fig. 3G). Together, these findings suggest a myeloid-restricted HSPC cell of origin for the *JAK2* V617F-mutated clone and *TET2* L1081*-mutated subclone, and distinct multipotent HSPC cells of origin for the separate *DNMT3A* R882C- and *GNAS* R844H-mutated clones.

Spatial Distribution of Hematopoietic Clones

To further characterize the spatial distribution of these hematopoietic clones in the bone marrow, the patient's femur head was partitioned into approximately 400 bone marrow fragments, of which 24 were selected for targeted panel DNA sequencing. These bone marrow fragments were sequenced using a myeloid panel (Supplementary Table S1). Variants were independently identified in each sample while retaining information on the spatial position for each fragment in the bone marrow. In the sequenced bone marrow fragments, the *JAK2* V617F mutation was identified in 24/24 fragments (0.12–0.69 VAF), the *TET2* L1081* mutation was identified in 11/24 fragments (0.03–0.05 VAF), and the *DNMT3A* R882C mutation was identified in 1/24 fragment (0.02 VAF; Supplementary Fig. S2A). The *GNAS* R844H mutation detected by single-cell sequencing was not identified in the bone marrow fragments using the gene panel sequencing approach (Supplementary Fig. S2A). In parallel, each mutation detected by bulk and single-cell sequencing was interrogated by ddPCR in 96 bone marrow fragments (including the 24 subjected to targeted sequencing), revealing significant spatial variability in mutational abundance (Fig. 4A). In contrast to targeted myeloid panel sequencing, which only identified the *TET2* L1081* (n = 11/24) and the *DNMT3A* R882C (n = 1/24) in a subset of fragments (Supplementary Fig. S2A), ddPCR identified each mutation in every assayed fragment (Fig. 4A). However, when a mutation was detected by both modalities, there was high concordance in VAF between ddPCR and sequencing (Supplementary Fig. S2B and S2C). To describe the spatial heterogeneity in clonal architecture across the tissue, hierarchical clustering of bone marrow fragments by normalized VAF, as determined by ddPCR, demonstrated four clusters (Fig. 4B; Supplementary Fig. S3). This clustering identified bone marrow fragments marked by high *JAK2* V617F and *TET2* L1081* VAF (cluster 2), representing increased prevalence of the neoplastic clone in that local bone marrow niche (Fig. 4C). Other clusters represented high prevalence of the *JAK2* V617F-mutant clone without *TET2* L1081* (cluster 3) and lower prevalence of any clones (clusters 1 and 2; Fig. 4C). Interestingly, the *GNAS* R844H and *DNMT3A* R882C-mutant clones were equally represented in clusters 1 and 2, suggesting that, although independent, these clones colocalized in the bone marrow with the neoplastic *JAK2* V617F-mutant clones (Fig. 4C). These clusters were also spatially constrained, representing contiguous areas with similar clonal composition (Fig. 4D). Imaging mass cytometry (IMC) analysis of bone marrow fragments from this individual also demonstrated clustering of $CD71^+$ cells (high *JAK2* V617F-mutant burden) separate from largely *JAK2* wild-type $CD15^+$ myeloid cells and $CD61^+$ megakaryocytes (Supplemen-

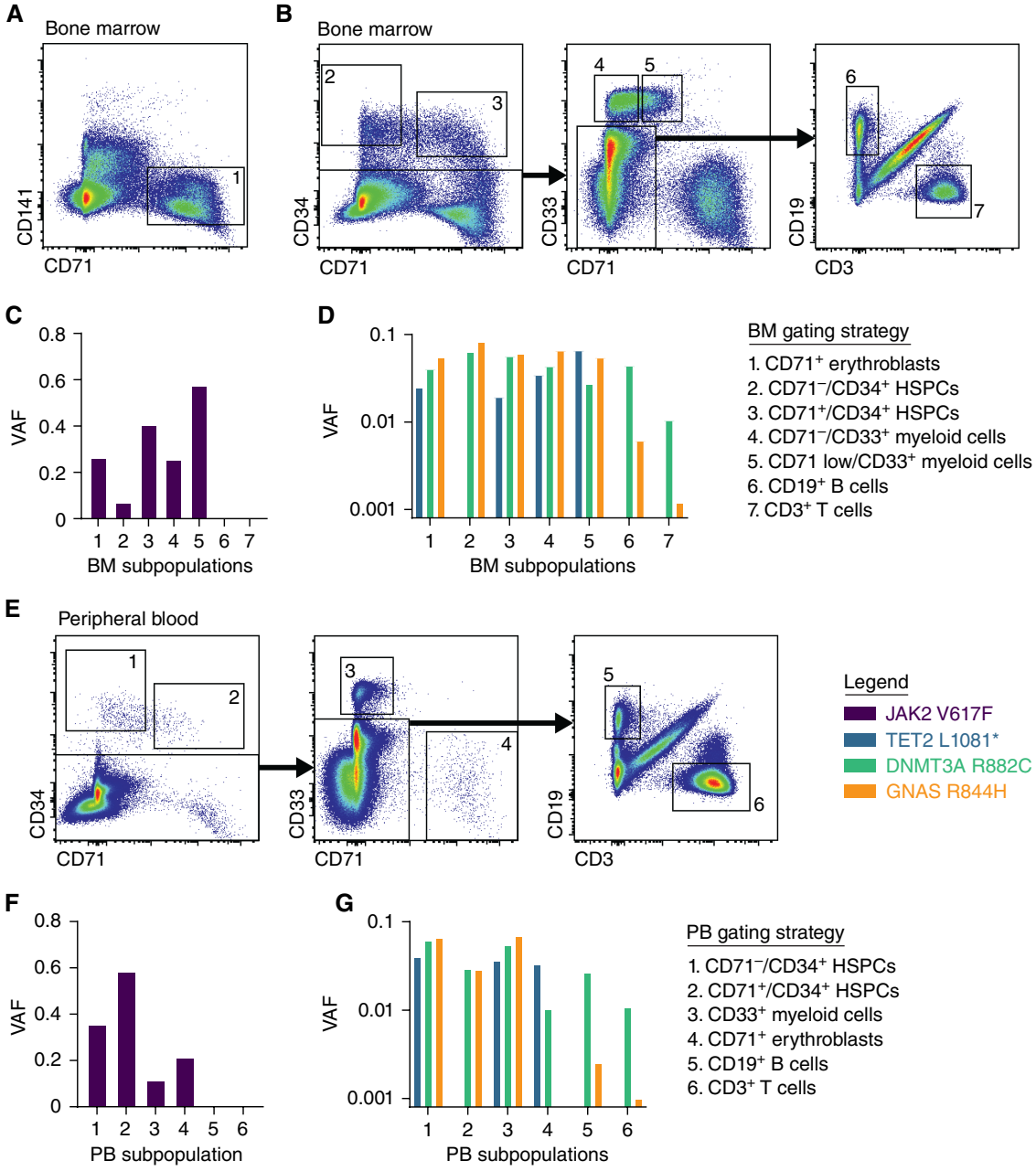

Figure 3. Mutation detection in HSPC subpopulations. **A,** Bone marrow flow cytometry gating to isolate CD71+ erythroblasts. **B,** Bone marrow flow cytometry gating to isolate other HSPC, myeloid, and lymphoid subpopulations. **C,** *JAK2* V617F VAF in sorted bone marrow subpopulations. **D,** *TET2* L1081*, *DNMT3A* R882C, and *GNAS* R844H VAF in sorted bone marrow subpopulations. **E,** Peripheral blood flow cytometry gating to isolate HSPC, CD71+ erythroblast, myeloid, and lymphoid subpopulations. **F,** *JAK2* V617F VAF in peripheral blood subpopulations. **G,** *TET2* L1081*, *DNMT3A* R882C, and *GNAS* R844H VAF in peripheral blood subpopulations. VAF, variant allele fraction.

tary Fig. S4). Together, this provides the first, to our knowledge, characterization of spatial distribution of clonal mutations in the human bone marrow niche.

DISCUSSION

Here, we present a novel method for spatially aware mutation detection in human bone marrow. Using this approach to characterize the spatial clonal distribution within the bone marrow of a patient with PV, we made several interesting and unexpected observations.

First, the clonal composition revealed by single-cell sequencing differed substantially from the one inferred by bulk sequencing. From the high VAF of *JAK2* V617F detected by bulk sequencing, the clinical interpretation was that a large proportion of the bone marrow cells were heterozygous for this mutation. But, the biology was more complex. Single-cell analysis revealed co-occurring *JAK2* V617F heterozygous and

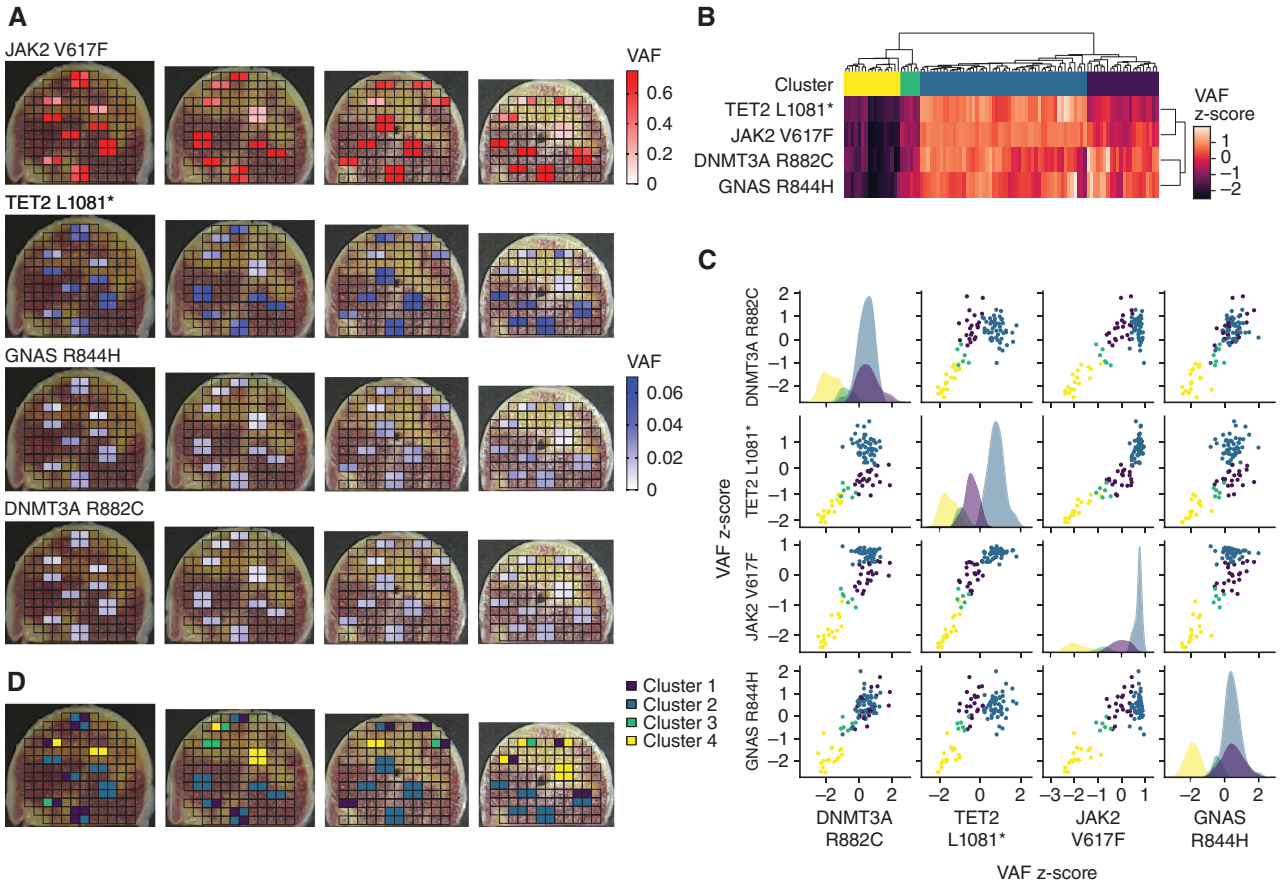

Figure 4. Spatial distribution of hematopoietic clones. **A,** Somatic mutations within 96 bone marrow fragments identified by ddPCR and color-coded by VAF. **B,** Clustering of individual bone marrow fragments by normalized somatic mutation VAF. **C,** Pairwise dot plots comparing VAF for each bone marrow fragment, color-coded by cluster identified in **B**. **D,** Overlay of bone marrow fragment clustering relative to position in the original tissue. VAF, variant allele fraction.

homozygous clones and a *TET2* L1081*-mutated subclone that likely contributed variably to the patient's disease, consistent with prior observations in the field (18). Moreover, mutations that initially appeared as *JAK2* V617F-mutated subclones by bulk sequencing (*DNMT3A* R882C and *GNAS* R844H) were actually in separate clones lacking the *JAK2* V617F mutation and likely did not contribute significantly to the patient's disease. This distinction was further supported by the bulk sequencing obtained a year after hip arthroplasty, showing the *JAK2* V617F and *TET2* L1081* mutations had increased, whereas the *GNAS* R844H and *DNMT3A* R882C mutations remained unchanged (Fig. 1A). These findings underscore the ever-evolving views of the genetic complexity of myeloid neoplasms.

Second, hematopoietic clones in the bone marrow were not well mixed. There were regions of high clonal diversity comprised of both the neoplastic and largely normal clones and separate regions of low clonal diversity. Within the bone marrow, there was considerable clonal variability within millimeters of marrow space. This highlights the complexity of making clinical management decisions for patients with hematologic malignancies from a single 2 mm core biopsy. Samples taken only millimeters apart had a vastly different representation of these malignant mutations. Future work will delve into understanding what bone marrow niche cell types and local microenvironment factors drive selection for local clonal expansion and evolution of specific mutations.

Third, the neoplastic cells identified by single-cell analysis showed high levels of CD141 and CD71, which has been observed previously in patients with PV (19). Additionally, normal hematopoietic markers were not expressed, aside from a small population of maturing progenitor cells marked by CD38. These findings highlight the limitations of using immunophenotype alone when detecting malignant disease, as there is variability in cell-surface phenotype across the population of cells marked by the same genetic drivers of disease. Additionally, the *DNMT3A* R882C and *GNAS* R844H clones were restricted to immature stem and progenitor cells. This is consistent with murine models that show a strong fitness effect and differentiation block for *DNMT3A* loss-of-function mutations in HSCs (20, 21). These independent lines of evidence support a model whereby *DNMT3A* mutations disrupt the balance between HSC self-renewal and differentiation. As such, inferring CH rates from peripheral blood analysis of mature circulating cells may vastly underestimate the clonal abundance in the bone marrow, particularly in immature HSPC populations (the presumptive disease-initiating cells).

This study is limited by only studying a single individual but is a critical proof of principle for this technique and analysis pipeline. Future work will expand this study to more

individuals with a wider array of malignant and nonmalignant hematologic conditions. The single-cell sequencing studies were limited by panel size, binding affinity of the immunophenotyping probes, and antigen prevalence/stability on the cells. Additionally, this study could not combine mutation detection with microscopic characterization in the same bone marrow fragment as the tissue was consumed during DNA extraction. Future work will seek to identify somatic mutations *in situ* while preserving the tissue for histologic characterization in the same cells.

In conclusion, we characterized the spatial distribution of clonal architecture in human bone marrow. We integrated bulk mutation detection, single-cell genotyping and immunophenotyping analysis, and spatial mutation detection to describe how these clones coexist within the bone marrow niche. Future applications of this platform will answer fundamental questions regarding how well hematopoietic clones mix in the bone marrow and further our understanding of the intrinsic and extrinsic factors governing local clonal evolution in the hematopoietic niche.

METHODS

Patient Selection

Peripheral blood, bone marrow, and femur head explant specimens were obtained from a patient (UPN978825) with PV after obtaining written informed consent in accordance with the Declaration of Helsinki ethical guidelines. The patient provided written informed consent for tissue banking and genomic analysis in accordance with protocol no. 201011766 approved by the Washington University in St. Louis Institutional Review Board. Human studies were approved by the Washington University Human Studies Committee (WU 01-1014).

Bone Marrow Partitioning

The femur head explant was obtained directly following hip arthroplasty and transported submerged in phosphate-buffered saline (Thermo Fisher Scientific). The femur head was sectioned into 2-mm slices using a band saw (Exakt 312 Pathology Saw). First, the specimen was leveled by sawing perpendicularly through the femur neck. Second, a 2-mm deep notch was introduced to approximate the middle of the flat surface made by the first step. Third, the specimen was sectioned into 2-mm–thick slices perpendicular to the notch created in the second step. This notch marked the bottom center of each slice to orient the sections. After sectioning, each slice was further partitioned into 2 mm^3 fragments using a combination of hand tools, including a bone chisel (Mopec), trimming blade (Sakura Finetek), and razor blade (VWR). Bone marrow fragments were stored in nontreated, sterilized 96-well plates (VWR) such that the location of each fragment was preserved relative to the original position in the slice. Likewise, bone marrow fragments that were adjacent in the original femur head slice were adjacent to the plate. A subset of fragments were selected for genomic DNA extraction, and the remainder were formalin-fixed and decalcified for imaging.

For the fragments selected for genomic DNA extraction, the bone marrow fragments were snap-frozen using liquid nitrogen in 1.5 mL microcentrifuge tubes (VWR). Frozen bone marrow fragments were pulverized in the microcentrifuge tube using a disposable pestle (USA Scientific). Genomic DNA was extracted as described below.

For the fragments selected for fixation, the bone marrow fragments were preserved using standard techniques (22). First, the fragments were submerged in 10% buffered formalin (Thermo Fisher Scientific) for 12 hours, after which the formalin was removed and the bone marrow fragments were decalcified using a 14% ethylenediaminetetraacetic acid (EDTA) solution, pH to 7.2 (Millipore Sigma). Bone marrow fragments were decalcified in EDTA that was changed every 3 to 4 days for 14 days total. After decalcification was complete, the samples were dehydrated in ethanol (Thermo Fisher Scientific). In this step, the samples were rinsed in deionized water (Millipore Sigma). Next, the samples were placed in 30% ethanol, then transferred to 50% ethanol, and finally transferred to 70% ethanol at room temperature for long-term storage.

Peripheral Blood and Bone Marrow Aspirate Processing

Peripheral blood and bone marrow aspirate were obtained perioperatively during hip arthroplasty. Mononuclear cells were isolated using SepMate tubes (STEMCELL Technologies) using their standard protocol. These mononuclear cells were isolated for genomic DNA extraction or viably frozen for single-cell sequencing. A subset of cells (5 million cell aliquots) were viably frozen in a 1:1 mixture suspended in Hanks' Balanced Salt Solution (HBSS; Corning) and freezing media. The freezing media were a 4:1 mixture of heat-inactivated fetal bovine serum (Thermo Fisher Scientific) and dimethyl sulfoxide (DMSO; Thermo Fisher Scientific). Cells were stored at −80°C for 24 hours and then transferred to liquid nitrogen for long-term storage.

Genomic DNA Extraction, Library Preparation, and Sequencing

Genomic DNA was isolated from pulverized bone marrow fragments, bulk peripheral blood, or bulk bone marrow aspirate using the PureLink Genomic DNA Mini Kit (Thermo Fisher Scientific). Genomic DNA was quantified using Qubit fluorometric quantification (Thermo Fisher Scientific). Libraries were prepared for targeted error-corrected sequencing using the Myeloseq assay (Supplementary Table S1) as described previously (23). Consensus reads were generated from read families with three or more reads sharing the same unique molecular index and mapped to the human reference genome (hg38) using version 3.10.4 of the DRAGEN pipeline (Illumina). Variants were annotated using Ensemble version 105 using VEP and COSMIC version 92 (16). Variants were filtered to exclude polymorphisms with >0.1% minor population allele frequency based on the gnomAD database version 2.1.1 (24).

Droplet Digital PCR (ddPCR)

Variants identified by bulk sequencing, bone marrow fragment sequencing, and single-cell sequencing were validated by ddPCR on the QX200 platform (Bio-Rad; ref. 25). For each sample, 20 to 50 ng of genomic DNA was utilized per reaction. Droplets were generated using the QX200 droplet generator (Bio-Rad) using their standard protocol. Droplets were PCR-amplified using the following thermocycler protocol: 95°C for 10 minutes, 40 cycles of 94°C for 30 seconds, 56°C for 1 minute, 98°C for 10 minutes, and 4°C hold. Droplets were analyzed on the QX200 droplet reader (Bio-Rad).

Single-Cell Sequencing and Immunophenotyping

Single-cell sequencing was performed using the Mission Bio Tapestri platform (26) using methods similar to previous single-cell studies of myeloid malignancies (27, 28). Cryovials of patient bone marrow were thawed, resuspended in HBSS, and quantified by cellometer (Nexcelom Bioscience). Cells were stained with 1:100 dilution of 7AAD viability staining solution (BioLegend) and live cells were isolated using a MoFlo cell sorter (Dako). One million live cells were suspended in cell staining buffer at 25,000 cells/μL. Cells were stained with the TotalSeq-D Heme Oncology Cocktail V1.0 (BioLegend) targeting 42 hematopoietic-specific proteins (Supplementary Table S3). After staining, the cells were washed with cell staining buffer and diluted to 3,000 to 4,000 cells/μL in cell buffer. Stained cells were encapsulated into microfluidic droplets using the Tapestri instrument, lysed, and barcoded for library amplification. Library

amplification utilized the Mission Bio myeloid panel targeting 45 genes with 312 amplicons that are recurrently mutated in myeloid malignancies (Supplementary Table S3; ref. 9). Afterward, the emulsions were broken and libraries were isolated by Ampure XP bead cleanup (Beckman Coulter). The protein libraries were enriched by biotinylated oligonucleotide bait pulldown. Each separate library underwent PCR amplification using sequencing primers containing library-specific indexes. Libraries were purified by Ampure XP bead cleanup. Library quality was assessed by TapeStation using the High Sensitivity D1000 ScreenTape (Agilent Technologies) and Qubit fluorescence quantification (Thermo Fisher Scientific). Libraries were sequenced on the Illumina NovaSeq 6000 platform using the 300-cycle kit targeting 173 million read pairs for the DNA myeloid panel and 150 million read pairs for the protein panel to ensure adequate coverage per panel for each cell captured.

FASTQ files containing the sequenced read information were analyzed using the cloud-based Tapestri Pipeline without modification. The pipeline trimmed the adapter sequences, mapped reads to the human reference genome (hg19) using BWA, and assigned reads to unique cells. Next, the GATK v4/Haplotypecaller was used to call genotypes for each cell. Variants were filtered using Tapestri Insights using the standard parameters (27). Somatic mutations were retained if they were observed in >1% of cells and were not likely to arise due to allelic dropout. Sequencing results were further normalized, clustered, and annotated using the Mission Bio Mosaic version 2.4. Figures were generated using the Mission Bio Mosaic v2.4 pipeline.

Cell Purification for Mutation Detection

Cryopreserved bone marrow and peripheral blood samples were thawed to 37°C and resuspended in HBSS buffer supplemented with 100 U/mL penicillin–streptomycin (Thermo Fisher Scientific) and 10 mmol/L HEPES (Thermo Fisher Scientific). The following antibodies were diluted 1:100 to stain the specimens for flow sorting: anti-human CD71 APC/Cy7 (clone CY1G4, BioLegend, no. 334110), anti-human CD141 BV421 (clone M80, BioLegend, no. 344113), anti-human CD34 PE (clone 561, BioLegend, no. 343606), anti-human CD33 BV605 (P67.6, BioLegend, no. 366611), anti-human CD19 FITC (clone 4G7, BioLegend, no. 392508), and anti-human CD3 PE/Cy7 (clone HIT3a, BioLegend, no. 300316). Flow-cytometric sorting was performed on the Cytek Aurora (Cytek Biosciences). Individual subpopulations of hematopoietic cells isolated by flow sorting were subsequently interrogated for somatic mutations by ddPCR using the methods described above.

Imaging Mass Cytometry

Bone marrow fragments selected for IMC were formalin-fixed and paraffin-embedded after decalcification using established protocols (22). IMC was conducted on sectioned bone marrow fragments using as previously described (29). The following cell-surface markers and isotope tags were utilized: 148Nd-CD71 (eBioscience, no. 14-0718-93, clone MRQ-48, 1:50), 164Dy-CD15 (Fluidigm, no. 3164001B, clone W6D3, 1:150), 160Gd-CD61 (Sigma-Aldrich, clone 2f2, 1:75), and 193Ir-DNA (Fluidigm, no. 201192A).

Data Availability Statement

The data generated in this study are publicly available in the National Center for Biotechnology Information Sequence Read Archive under the BioProject accession number PRJNA1074831.

Authors' Disclosures

A.L. Young reports grants from the American Society of Hematology Research Training Award for Fellows during the conduct of the study and personal fees from BioGenerator outside the submitted work. T.M. Parsons reports personal fees from MPN Research Foundation outside the submitted work. L. Sun reports personal fees from the Association for Molecular Pathology outside the submitted work. S.T. Oh reports personal fees from Kartos, CTI Biopharma, Celgene/Bristol Myers Squibb, Disc Medicine, Blueprint Medicines, PharmaEssentia, Constellation, Geron, AbbVie, Sierra Oncology, and Incyte outside the submitted work. G.A. Challen reports grants from Incyte and Ajax Therapeutics and personal fees from ReNAgade Therapeutics Management outside the submitted work. No disclosures were reported by the other authors.

Authors' Contributions

A.L. Young: Conceptualization, data curation, formal analysis, validation, investigation, visualization, methodology, writing–original draft, writing–review and editing. **H.C. Davis:** Conceptualization, investigation, writing–review and editing. **M.J. Cox:** Resources, writing–review and editing. **T.M. Parsons:** Investigation, writing–review and editing. **S.C. Burkart:** Investigation, writing–review and editing. **D.E. Bender:** Investigation, writing–review and editing. **L. Sun:** Conceptualization, resources, writing–review and editing. **S.T. Oh:** Resources, supervision, writing–review and editing. **G.A. Challen:** Conceptualization, resources, supervision, funding acquisition, project administration, writing–review and editing.

Acknowledgments

We thank all members of the Challen laboratory for ongoing contributions and critical discussion. We thank the Siteman Cancer Center Flow Cytometry Core, which is supported by NIH Cancer Center Support Grant P30CA091842. Support for the procurement of human samples was provided by the Genomics of AML Program Project Grant P01 CA101937 to Dr. Timothy Ley. Support for assay development was provided by the Edward P. Evans Center for Myelodysplastic Syndromes at Washington University and the Foundation for Barnes-Jewish Hospital Cancer Frontier Fund (5109) to Dr. Matt Walter. We thank Mary Anthes-Bartlow and Abigail Bogle for assistance with sample handling and processing. We thank Dr. David Spencer and Dr. Eric Duncavage for bioinformatics analysis expertise. We thank Dr. Stephen Sykes and Dr. Francesca Ferraro for technical expertise. This publication is solely the responsibility of the authors and does not necessarily represent the official views of the NIH. G.A. Challen was supported by the NIH (NIH; HL147978, CA236819, and DK124883), the American Cancer Society (CSCC-RSG-23–991417–01-CSCC), and the Edward P. Evans Foundation. S.T. Oh was supported by the NIH (HL134952, HL150636), MPN Research Foundation, Leukemia and Lymphoma Society Translational Research Program, and When Everyone Survives Foundation. T.M. Parsons was a fellow of the Leukemia and Lymphoma Society. A.L. Young was supported by NIH T32HL007088 and the ASH Research Training Award for Fellows. G.A. Challen was a scholar of the Leukemia and Lymphoma Society.

Note

Supplementary data for this article are available at Blood Cancer Discovery Online (https://bloodcancerdiscov.aacrjournals.org/).

Received June 26, 2023; revised November 21, 2023; accepted February 26, 2024; published first March 14, 2024.

REFERENCES

1. Colom B, Herms A, Hall MWJ, Dentro SC, King C, Sood RK, et al. Mutant clones in normal epithelium outcompete and eliminate emerging tumours. Nature 2021;598:510–4.
2. Martincorena I, Roshan A, Gerstung M, Ellis P, Van Loo P, McLaren S, et al. Tumor evolution: high burden and pervasive positive selection of somatic mutations in normal human skin. Science 2015;348:880–6.
3. Steensma DP, Bejar R, Jaiswal S, Lindsley RC, Sekeres MA, Hasserjian RP, et al. Clonal hematopoiesis of indeterminate potential and its distinction from myelodysplastic syndromes. Blood 2015;126:9–16.

4. Watson CJ, Papula AL, Poon GYP, Wong WH, Young AL, Druley TE, et al. The evolutionary dynamics and fitness landscape of clonal hematopoiesis. Science 2020;367:1449–54.
5. Young AL, Challen GA, Birmann BM, Druley TE. Clonal haematopoiesis harbouring AML-associated mutations is ubiquitous in healthy adults. Nat Commun 2016;7:12484.
6. Genovese G, Kahler AK, Handsaker RE, Lindberg J, Rose SA, Bakhoum SF, et al. Clonal hematopoiesis and blood-cancer risk inferred from blood DNA sequence. N Engl J Med 2014;371:2477–87.
7. Jaiswal S, Fontanillas P, Flannick J, Manning A, Grauman PV, Mar BG, et al. Age-related clonal hematopoiesis associated with adverse outcomes. N Engl J Med 2014;371:2488–98.
8. Xie M, Lu C, Wang J, McLellan MD, Johnson KJ, Wendl MC, et al. Age-related mutations associated with clonal hematopoietic expansion and malignancies. Nat Med 2014;20:1472–8.
9. Papaemmanuil E, Gerstung M, Bullinger L, Gaidzik VI, Paschka P, Roberts ND, et al. Genomic classification and prognosis in acute myeloid leukemia. N Engl J Med 2016;374:2209–21.
10. Cancer Genome Atlas Research N, Ley TJ, Miller C, Ding L, Raphael BJ, Mungall AJ, et al. Genomic and epigenomic landscapes of adult de novo acute myeloid leukemia. N Engl J Med 2013;368:2059–74.
11. Hecker JS, Hartmann L, Riviere J, Buck MC, van der Garde M, Rothenberg-Thurley M, et al. CHIP and hips: clonal hematopoiesis is common in patients undergoing hip arthroplasty and is associated with autoimmune disease. Blood 2021;138:1727–32.
12. Osman AEG, Mencia-Trinchant N, Saygin C, Moma L, Kim A, Housman G, et al. Paired bone marrow and peripheral blood samples demonstrate lack of widespread dissemination of some CH clones. Blood Adv 2023;7:1910–4.
13. Levine RL, Wadleigh M, Cools J, Ebert BL, Wernig G, Huntly BJ, et al. Activating mutation in the tyrosine kinase JAK2 in polycythemia vera, essential thrombocythemia, and myeloid metaplasia with myelofibrosis. Cancer Cell 2005;7:387–97.
14. Young AL, Tong RS, Birmann BM, Druley TE. Clonal hematopoiesis and risk of acute myeloid leukemia. Haematologica 2019;104:2410–7.
15. Williams N, Lee J, Mitchell E, Moore L, Baxter EJ, Hewinson J, et al. Life histories of myeloproliferative neoplasms inferred from phylogenies. Nature 2022;602:162–8.
16. Tate JG, Bamford S, Jubb HC, Sondka Z, Beare DM, Bindal N, et al. COSMIC: the catalogue of somatic mutations in cancer. Nucleic Acids Res 2019;47:D941–7.
17. Ostrander EL, Koh WK, Mallaney C, Kramer AC, Wilson WC, Zhang B, et al. The GNAS(R201C) mutation associated with clonal hematopoiesis supports transplantable hematopoietic stem cell activity. Exp Hematol 2018;57:14–20.
18. Godfrey AL, Nangalia J, Baxter EJ, Massie CE, Kent DG, Papaemmanuil E, et al. Nongenetic stochastic expansion of JAK2V617F-homozygous subclones in polycythemia vera? Blood 2014;124:3332–4.
19. Shahrabi S, Ehsanpour A, Heidary S, Shahjahani M, Behzad MM. Expression of CD markers in JAK2(V617F) positive myeloproliferative neoplasms: prognostic significance. Oncol Rev 2018;12:373.
20. Challen GA, Sun D, Jeong M, Luo M, Jelinek J, Berg JS, et al. Dnmt3a is essential for hematopoietic stem cell differentiation. Nat Genet 2011;44:23–31.
21. Jeong M, Park HJ, Celik H, Ostrander EL, Reyes JM, Guzman A, et al. Loss of Dnmt3a immortalizes hematopoietic stem cells in vivo. Cell Rep 2018;23:1–10.
22. Idleburg C, Lorenz MR, DeLassus EN, Scheller EL, Veis DJ. Immunostaining of skeletal tissues. Methods Mol Biol 2021;2221:261–73.
23. Duncavage EJ, Jacoby MA, Chang GS, Miller CA, Edwin N, Shao J, et al. Mutation clearance after transplantation for myelodysplastic syndrome. N Engl J Med 2018;379:1028–41.
24. Karczewski KJ, Francioli LC, Tiao G, Cummings BB, Alfoldi J, Wang Q, et al. The mutational constraint spectrum quantified from variation in 141,456 humans. Nature 2020;581:434–43.
25. Hindson BJ, Ness KD, Masquelier DA, Belgrader P, Heredia NJ, Makarewicz AJ, et al. High-throughput droplet digital PCR system for absolute quantitation of DNA copy number. Anal Chem 2011;83:8604–10.
26. Pellegrino M, Sciambi A, Treusch S, Durruthy-Durruthy R, Gokhale K, Jacob J, et al. High-throughput single-cell DNA sequencing of acute myeloid leukemia tumors with droplet microfluidics. Genome Res 2018;28:1345–52.
27. Miles LA, Bowman RL, Merlinsky TR, Csete IS, Ooi AT, Durruthy-Durruthy R, et al. Single-cell mutation analysis of clonal evolution in myeloid malignancies. Nature 2020;587:477–82.
28. Morita K, Wang F, Jahn K, Hu T, Tanaka T, Sasaki Y, et al. Clonal evolution of acute myeloid leukemia revealed by high-throughput single-cell genomics. Nat Commun 2020;11:5327.
29. Lu P, Oetjen KA, Bender DE, Ruzinova MB, Fisher DAC, Shim KG, et al. IMC-Denoise: a content aware denoising pipeline to enhance imaging mass cytometry. Nat Commun 2023;14:1601.